How to cite: *Angew. Chem. Int. Ed.* **2023,** *62,* e202211946
International Edition: doi.org/10.1002/anie.202211946
German Edition: doi.org/10.1002/ange.202211946

Ladder Polymers

Circularly Polarized Light Probes Excited-State Delocalization in Rectangular Ladder-type Pentaphenyl Helices

Robin Ammenhäuser, Patrick Klein, Eva Schmid, Sabrina Streicher, Jan Vogelsang, Christian W. Lehmann, John M. Lupton, Stefan C. J. Meskers, and Ullrich Scherf*

Abstract: Ladder-type pentaphenyl chromophores have a rigid, planar π-system and show bright fluorescence featuring pronounced vibrational structure. Such moieties are ideal for studying interchromophoric interactions and delocalization of electronic excitations. We report the synthesis of helical polymers with a rigid square structure based on spiro-linked ladder-type pentaphenyl units. The variation of circular dichroism with increasing chain length provides direct evidence for delocalization of electronic excitations over at least 10 monomeric units. The change in the degree of circular polarization of the fluorescence across the vibronic side bands shows that vibrational motion can localize the excitation dynamically to almost one single unit through breakdown of the Born-Oppenheimer approximation. The dynamic conversion between delocalized and localized excited states provides a new paradigm for interpreting circular dichroism in helical polymers such as proteins and polynucleic acids.

[*] R. Ammenhäuser, Dr. P. Klein, Prof. Dr. U. Scherf
Department of Chemistry, Macromolecular Chemistry group (BUW-makro), and Wuppertal Institute for Smart Materials and Systems (CM@S), Bergische Universität Wuppertal
Gauss-Str. 20, 42119 Wuppertal (Germany)

E. Schmid, S. Streicher, Dr. J. Vogelsang, Prof. Dr. J. M. Lupton
Institut für Experimentelle und Angewandte Physik, Universität Regensburg
Universitätsstrasse 31, 93053 Regensburg (Germany)

Prof. Dr. C. W. Lehmann
Max-Planck-Institut für Kohlenforschung
Kaiser-Wilhelm-Platz 1, 45470 Mülheim an der Ruhr (Germany)

Dr. S. C. J. Meskers
Molecular Materials and Nanosystems and Institute of Complex Molecular Systems, Technische Universiteit Eindhoven
PO Box 513, 5600 MB Eindhoven (The Netherlands)
E-mail: s.c.j.meskers@tue.nl

Introduction

The conformation of biomacromolecules such as polynucleic acids and polypeptides is key to understanding their biological activity. One of the main tools to study their conformation, or secondary structure, is circular dichroism (CD) spectroscopy. A major question in the interpretation of CD spectra is how the optical characteristics associated with a particular secondary structural element, e.g. an α-helix, vary with the length of the structural element. It is well appreciated that the CD results primarily from excitonic coupling between various chromophoric groups held in a chiral arrangement by the backbone of the polymer.[1] Exitonic coupling promotes delocalization of excited states over several groups, implying a sensitivity of CD to long- range structural order in the macromolecule. At the same time, variation in the structure and also vibrational motion tends to localize excitations, suggesting that CD can only offer information on short-range structural order.

Over the past decade a new paradigm has emerged for the interpretation of CD spectra, where also the coupling between electronic and vibrational degrees of freedom, i.e., the deviation from the Born-Oppenheimer approximation, is taken into account. Coupling between electronic and vibrational motion, also referred to as vibronic coupling, can lead to *dynamic* localization of excitations, where the excitation "breathes" during the cycle of zero-point nuclear motion in the excited state.[2] Dynamic localization thus allows for a spectrum associated with a particular excited state to display, paradoxically, features indicative of both a localized and a delocalized nature of the excited state involved. This localization opens new possibilities for correlating experimental spectra to the structural content of the macromolecule under study.

For peptides and proteins the importance of the interdependence of electronic and vibrational excitation in interpretation of the shape of CD spectral bands has been realized in the past decades.[3] Also for nucleic acids the role of so-called non-adiabatic coupling between electron and nuclear motion for understanding the CD and the photophysics in general has gained wider appreciation.[4] However, a major difficulty in addressing the fundamental issue of delocalization of the excited states is that for most biomacromolecules, the excited states involved lie deep in the UV spectral range and are very closely spaced in energy. As a result, the experimental spectra of the biopolymers show only highly convoluted spectral features precluding

detailed experimental verification of the predictions for the combined motion of electrons and nuclei upon excitation.

Rigid helices of high structural stability are widely realized in nature, as in double-stranded DNA or peptide helices. From the perspective of synthetic polymer chemistry, however, it is rather challenging to create artificial, shape-persistent polymeric helices that contain extended π-conjugated segments held together exclusively by strong covalent bonds of a ladder-type framework rather than weak H-bonds or dispersive forces in supramolecular arrangements. A few examples of such rigid ladder helices have been reported: Takata and co-workers reported the syntheses of squared helical coordination ladders[5] by metal complexation as well as of helical ladder polymers made in nucleophilic aromatic substitutions as the cyclization step.[6] Swager and co-workers reported the generation of ladderized helices with chiral triptycene knots made in an electrophilic post-polymerization cyclization step between the main chain aromatic units and the ethynyl substituents.[7] Yashima and co-workers recently described helical ladder polymers with chiral spirobisindane linkers.[8] In addition, sophisticated theoretical methods have been developed to describe the effect of non-adiabatic coupling, and these have highlighted the importance of electron-vibrational coupling in the photophysics of polyfluorene-type polymers.[9]

The objectives of our present study are the synthesis and characterization of structurally optimally defined, helical ladder polymers with a maximum degree of rigidity as well as a fully defined orientation of the π-electron planes of their conjugated segments in space and in relation to the axis of the helix. The ladders are made by connecting planar pentaphenyl segments through enantiopure 9,9′-spirobifluorene linkers. These rigid π-conjugated ladder polymers feature highly resolved optical transitions associated with excitation of the backbone in an easily accessible spectral region. Moreover, the polymers are also fluorescent, which allows us to use circularly polarized luminescence (CPL) to study the lower excited states in more detail.[10] The individual ladder segments of the polymer are rigid and are forced to retain their flat structure whereas the stereocentres at the spiro linkages between these segments force the monomeric units into a defined helical arrangement. As a result, the CPL directly reflects the degree of delocalization of the photoexcitation between the pentafluorene segments of the helical polymer. This correlation allows us to examine the degree of delocalization of the excited state along the polymer backbone by using polarization-resolved spectroscopy. The CD and CPL spectra of the polymers show a clear evolution with the length of the polymer beyond the helical repeat length, providing direct evidence for a high degree of delocalization. However, these length-dependent features occur close to the onset of absorption and emission and are suppressed for the higher-order vibronic transitions. These observations argue for a description where the excited states are delocalized during part of the excited-state zero-point vibrational motion when the nuclear modes coupling to the excitation are near their equilibrium amplitude. During other parts of the vibrational cycle, the excitation is localized dynamically through the temporary distortion of the nuclear geometry induced by the vibrational motion. We detail this interpretation with a quantum-mechanical model that goes beyond the Born-Oppenheimer approximation.

Results and Discussion

The availability of the enantiopure 2,2′-diiodo-9,9′-spirobifluorene building block (**5**) requires the regioselective introduction of two halogen substituents at 2- and 2′-positions of the 9,9′-spirobifluorene (**1**) core as well as an enantiomeric separation.[12] Since the latter was not practical after a direct halogenation of the 9,9′-spirobifluorene (1) core due to the presence of low polarity educts and products, an indirect synthesis[11] (Scheme 1) was used instead. The first step is a twofold nitration followed by reduction to diamine **3**, which is then converted into the diiodo derivative **5** in a Sandmeyer-type reaction. Alternatively, **3** can be converted to the diborylated compound **4**, which proved to be less practical due to the lower yield. For separation of enantiomers by HPLC, **4** and **5** proved to be unsuitable because of their lower polarity. Therefore, the diamino precursor **3** was used instead (see Figure S19 in the Supporting Information). The first eluted enantiomer was assigned to be the (*R*)-enantiomer by its X-ray crystal structure,[12] thus the secondly eluted enantiomer must be the (*S*)-enantiomer.

With this approach, helical ladder polymers as well as ladderized dimers were synthesized (Scheme 2). In addition to polymer synthesis (**SBF-LPP**, Scheme 2, right), corresponding model dimers (**SBF-LOP**) were synthesized, with only 4 instead of 5 phenyl units in conjugation owing to their easier accessibility. For the synthesis of the model compounds, the first step is a Suzuki–Miyaura cross-coupling between (*rac*)-**5** and the monofunctional endcapper **6** into (*rac*)-**SBF-LOP-O**. The racemic mixture was subsequently

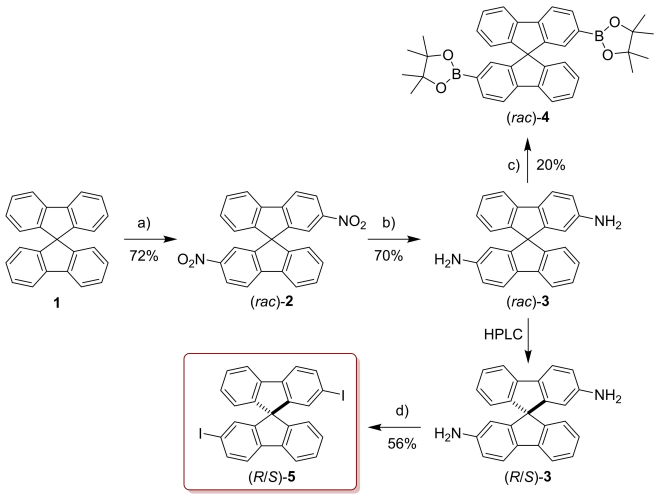

Scheme 1. Synthesis of **5**. a) HNO_3, AcOH, 120 °C, 6 h. b) H_2 (2.3 bar), [Pd/C], EA/EtOH (10/1), rt, 4 d. c) B_2pin_2, *t*-butyl nitrite, MeCN, 80 °C, 5 h. d) 1. $NaNO_2$, H_2O/HCl (3/1), < 0 °C, 20 min; 2. KI, H_2O/HCl (4/1), < 0 °C→80 °C, 3 h.

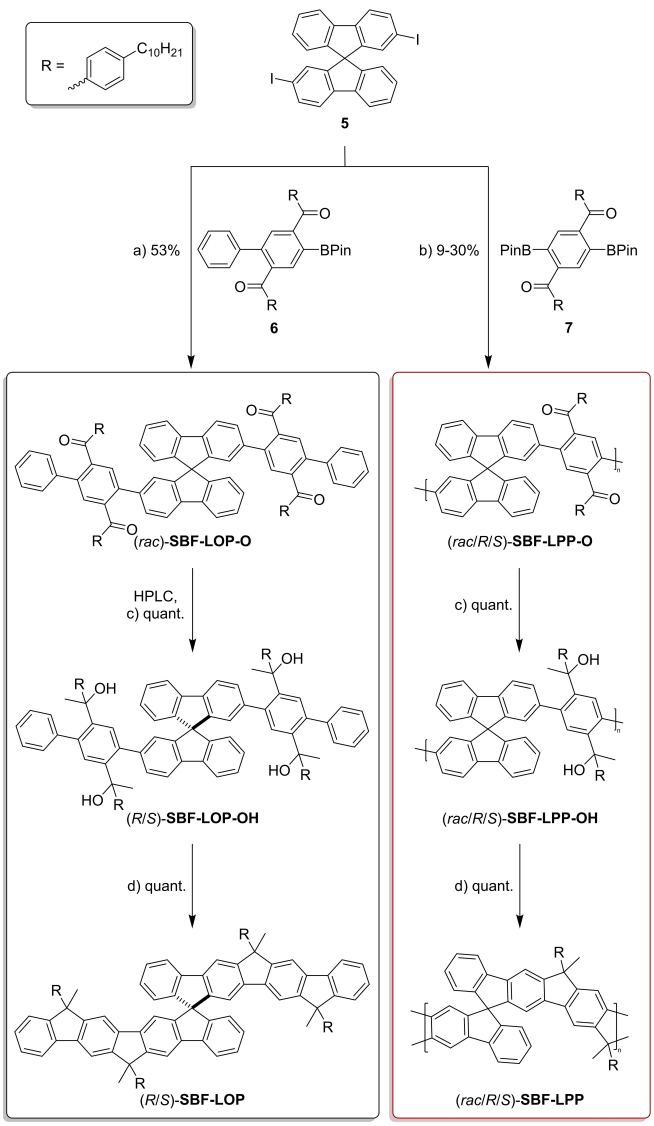

Scheme 2. Synthesis of **SBF-LOP** (black box) and **SBF-LPP** (red box). a) K_2CO_3, [$Pd(PPh_3)_4$], THF/H_2O (4/1), 75 °C, 1 d. b) Cs_2CO_3, [$Pd(PPh_3)_4$], THF/H_2O (4/1), 75 °C, 3 d. c) MeLi, toluene, 0 °C→rt, 16 h. d) $BF_3{\cdot}OEt_2$, DCM, rt, 16 h.

separated into the pure enantiomers by enantioselective HPLC (Figure S20 in the Supporting Information), as a higher enantiomeric purity could be achieved with the chromatographic purification at this stage. For polymerization, the difunctional comonomer **7** was used instead of **6**, and the polycondensation was carried out both for enantiopure and racemic **5**. The respective dimeric ketones or polyketones were subsequently converted into the corresponding tertiary alcohols by reduction with methyl lithium in nearly quantitative yield, and finally ladderized by ring closure with boron trifluoride diethyl etherate. The two-step ladderization sequence produces one asymmetric carbon per methylene bridge. It is assumed that the fourfold cyclization towards the dimers **SBF-LOP** leads to an arbitrary arrangement of the corresponding four chiral carbon centers. However, for the two helical ladder polymers (*R*)-**SBF-LPP** and (*S*)-**SBF-LPP** we expect a preferential orientation of the bulkier 4-*n*-decylaryl substituents -R towards the outside of the helices. This assumption is based on simple considerations of space occupation.

Table 1 summarizes molecular weight (MW) data and photoluminescence (PL) quantum yields of the ladder polymers and dimeric model compounds. The low-molecular-weight acetone fractions (collected by Soxhlet extraction) **SBF-LPP-A** show molecular weights (M_n) of 4.6–5.2 kg mol^{-1}, which corresponds to a degree of polymerization (P_n) of 5–6 repeat units. In the case of the helical polymers (*R*)-**SBF-LPP-A** and (*S*)-**SBF-LPP-A**, this corresponds to helices with approximately 1.5 turns. In contrast, the chloroform fractions **SBF-LPP-C** show molecular weights of 8.7–12.2 kg mol^{-1}, corresponding to 10–14 repeat units or, on average, 2.5–3.5 helix turns. All polymers show medium-high PL quantum yields of 52–63 % (Φ, PLQY) in solution. While the absolute configuration (*rac, R* or *S*) is of insignificant influence on the PL quantum yield, some decrease with increasing chain length can be observed, as expected, since intrachain excitation energy transfer to quenching defect sites becomes more probable in longer chains.[13] The higher MW **SBF-LPP-C** has a quantum yield of roughly 53 %, which increases to 59 % for the lower MW **SBF-LPP-A** and to 86 % in the model dimer **SBF-LOP**.

The fluorescence spectra of **SBF-LOP** and **SBF-LPP**, see Figure 1, show all the features characteristic of ladder-type oligophenyl-based chromophores: clearly resolved vibronic structure in excitation and emission, mirror image symmetry between PLE and fluorescence spectra, and a very small Stokes shift of only c. 30 meV (**SBF-LOP**) or 40 meV (**SBF-LPP**). In **SBF-LOP**, the three main transitions are at 3.33, 3.50 and 3.68 eV (PLE) and 3.30, 3.12 and 2.94 eV (PL) with the 0–0 transitions as global maxima. As expected, the polymer spectra display similar spectral shapes, but are bathochromically shifted due to the elongation of the conjugated system (5 vs. 4 phenyls), with transitions at 3.14, 3.32, 3.49 eV (PLE) and 3.10, 2.91, 2.73 eV (PL). In **SBF-LPP**, there is only a very small interaction of the π-orbitals via the spirobifluorene linkage, for which the conjugation is mainly restricted to individual pentaphenyl units.

Table 1: Molecular weight (MW) data and PL quantum yields of the ladderized compounds.

Compound	M_n [kg mol^{-1}]	M_w [kg mol^{-1}]	P_n	PDI	Yield [%]	Φ [%][a]
(*rac*)-**SBF-LPP-C**	8.7	12.0	10	1.4	30	54
(*R*)-**SBF-LPP-C**	12.2	18.9	14	1.5	28	53
(*S*)-**SBF-LPP-C**	9.6	12,3	11	1.3	9	52
(*rac*)-**SBF-LPP-A**	4.6	7.0	5	1.5	65	63
(*R*)-**SBF-LPP-A**	5.2	7.1	6	1.4	59	56
(*S*)-**SBF-LPP-A**	5.0	6.7	6	1.4	84	59
(*R*)-**SBF-LOP**	–	–	–	–	–	85
(*S*)-**SBF-LOP**	–	–	–	–	–	86

[a] measured in cyclohexane at room temperature and referenced to 1,4-bis(5-phenyloxazol-2-yl)benzene (**POPOP**), precision ±5%.

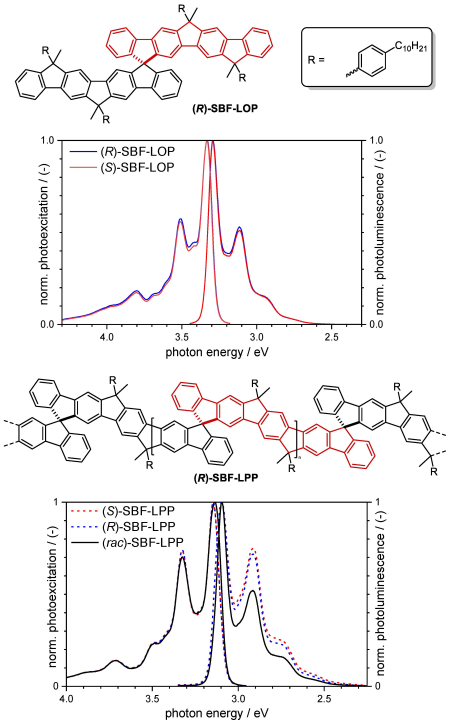

Figure 1. Normalized PL excitation (PLE) and luminescence spectra of **SBF-LOP** (upper) and **SBF-LPP** (lower) (solvent: THF at 25 °C).

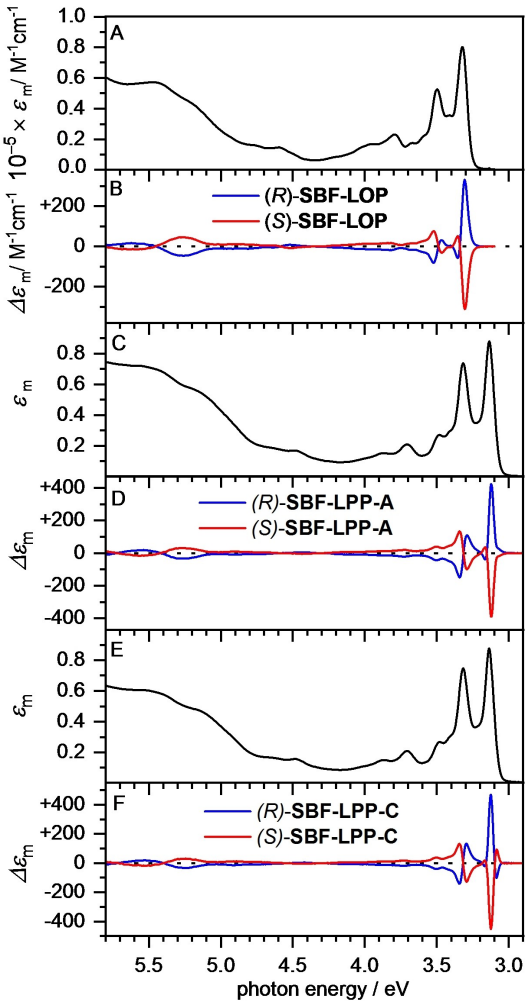

Figure 2. Absorption (A) and CD spectra (B) of **SBF-LOP** in THF at 25 °C. C), D) and E), F) show corresponding data for **SBF-LPP-A** and **SBF-LPP-C**. ε_m denotes the absorption coefficient per monomeric unit.

Figure 2 compares the absorption and CD spectra of the model compound **SBF-LOP** with those of the polymer fractions **SBF-LPP-C** and **SBF-LPP-A**. Since the absorption spectra of respective enantiomers are almost identical, for simplicity, we show only the spectra of the (*R*)-enantiomers. In contrast, the CD spectra show mirror symmetry with different signs of the respective bands for the two enantiomers. The mirror symmetry of the spectra proves that, in effect, two enantiomers of chemically otherwise identical compounds are present. We therefore only discuss the spectra of the (*R*)-enantiomers in the following, with the (*S*)-enantiomers showing the inverse values.

All compounds show a distorted couplet in the region of the 0–0 transition with the long-wavelength positive lobe emerging as the more intense band. The 0–1 transitions also exhibit bisignate Cotton effects with the inflection point close to the respective absorption maxima. However, some differences between the two Soxhlet-extracted fractions of the polymers are apparent. The lower MW **SBF-LPP-A** as well as dimer **SBF-LOP** show very similar $g_{abs} = \Delta\varepsilon / \varepsilon = (\varepsilon_L - \varepsilon_R)/\varepsilon$ values with maxima of $+5.0\times10^{-3}$ (3.12 eV, see Figure 3) and $+4.9\times10^{-3}$ (3.28 eV), respectively, whereas the higher MW polymer fraction **SBF-LPP-C** shows an increase of g_{abs} to a maximum value of $+5.9\times10^{-3}$. Importantly, for **SBF-LPP-C** an additional CD band arises at 3.08 eV (Figure 2), which is not present for the other derivatives. This additional CD band is further characterized by $g_{abs} = -4.2\times10^{-3}$, with the sign opposite to that of the main band. This inversion indicates that the CD spectra are distinctly influenced by the formation of the helical structure. Such a helix-related amplification of the CD response with increasing chain length has previously been found for polypeptides,[14] and concluded from the influence of the molecular weight on g_{abs} for so-called artificial chiral ladders.[7,8] There is no significant influence of temperature and concentration on the effects described (see Figure S23 in the Supporting Information). The perpendicular arrangement of constituent chromophores enforced by the spiro linkages suppresses aggregation of polymer chains. However, addition of a highly polar solvent does indeed induce a distinct decrease of the $|g_{abs}|$ values, which is likely due to the conglomeration of chains. On the other hand, the addition of a polar solvent does not lead to significant changes in the spectral shapes (Figure S24). This finding therefore excludes aggregation effects as the source of the observed MW-dependent CD effects, implying that it is monomolecular in nature.

The maximum $|g_{abs}|$ value of **SBF-LPP-C** of 5.9×10^{-3} is comparable to that of other helical ladder polymers. The spirobisindane-bridged ladder polymers of Yashima and co-

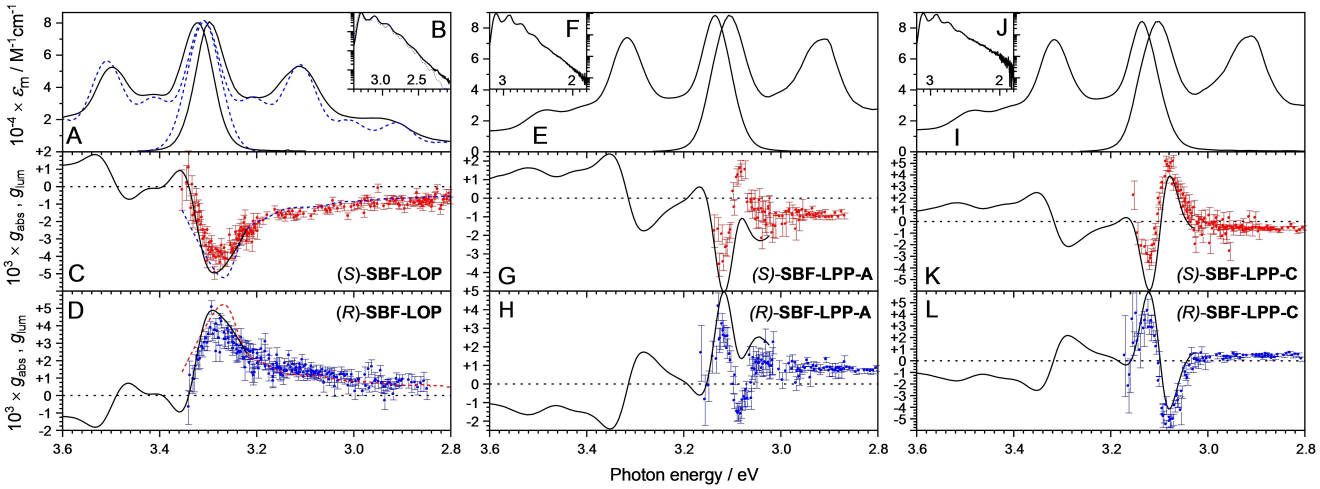

Figure 3. A), B) Absorption and fluorescence for (*S*)-**SBF-LOP** in THF (black). The dashed blue lines show the results from quantum-mechanical model calculations assuming two totally symmetric active vibrations, one with 1600 cm^{-1} frequency and a Huang–Rhys factor $S=0.6$ with up to 8 quanta, and the other at 820 cm^{-1}, $S=0.39$, with up to 3 quanta. (C,D) Dissymmetry factor for circular polarization in absorption g_{abs} (back) and luminescence g_{lum} (symbols with error bars) for (*S*)-**SBF-LOP** (C, red) and (*R*)-**SBF-LOP** (D, blue) in THF. Dashed lines show the predictions from the quantum-mechanical model for g_{lum}. E–H) and I–L) show corresponding data for **SBF-LPP-A** and **SBF-LPP-C**.

workers[8] and the triptycene-based ladders of Swager and co-workers[7] show slightly lower extremal $|g_{abs}|$ values of 2.7×10^{-3} and 4.1×10^{-3}, respectively. Also for the dimeric model compounds of these chiral polymers it holds that spirobisfluorene has a degree of circular polarization comparable to the other models (**SBF-LOP**: max. $|g_{abs}|=5\times10^{-3}$ vs. 1.6×10^{-3} and 1.8×10^{-3} for the bisindane and triptycene models, respectively.[7] Notably, these dissymmetry factors are more than an order of magnitude smaller than the extrema reported for thermally annealed films of chiral fluorene-based polymers.[15]

We analyze the molecular weight effects in more detail in Figure 4. When comparing normalized CD spectra close to the onset of absorption (3.04–3.16 eV) for a series of polymer fractions with different degree of polymerization *n*, we notice the following. For the shortest fragment g_{abs} reaches its most negative value at 3.12 eV. With increasing molecular weight the minimum first shifts to lower photon energies, but then for *n* exceeding 4, the minimum shifts back again to higher photon energies. For polymers with *n* exceeding ≈8, a new CD band with a positive sign appears at 3.09 eV. The maximum $|g_{abs}|$ values are reached for roughly 20 repeat units (5 helical turns, see Figure S25). A similar number for this saturation limit was found by Zheng et al.[8] for their chiral ladder polymers.

To understand these length-dependent features in the CD spectra in more detail, we turn to the CPL. We begin with the enantiomers of the dimeric model compounds **SBF-LOP**, see Figure 3. The fluorescence from these molecules is circularly polarized with a degree of circular polarization $g_{lum}=2(I_L-I_R)/(I_L+I_R)$ equal to $+4.0\times10^{-3}$ near the 0–0 band, i.e. at 3.28 eV for the *R*-enantiomer. The sign and magnitude of g_{lum} for both enantiomers correspond closely to g_{abs} at the same photon energy, see Figure 3C,D. Interestingly, for the higher vibronic transitions in the fluorescence spectrum we find that the circular polarization is strongly suppressed, *viz.* $g_{lum}=+1.5\times10^{-3}$ at 3.1 eV near the 0–1 feature in the PL spectrum (Figure 3A).

The coupled electronic oscillator picture, or exciton model, provides insight into this curious wavelength dependence of the CPL. In the exciton model two achiral chromophores are held in a chiral arrangement by a molecular scaffold. The circular polarization derives directly from delocalization of the excitation over the two chromophores and provides important information on the absolute stereochemistry of the molecular scaffold holding the two chromophores. Extending this argument, the reduction in g_{lum} values for the higher vibronic transitions in comparison to the spectral region of the 0–0 transition shows that in the nuclear geometries that contribute to the higher-order vibronic transitions the electronic excitation is more localized to a single-chromophore unit. In contrast, in the nuclear geometries giving rise to the 0–0 transition, the electronic excitation must be spread more evenly over the two orthogonal chromophores. Evidence for such an orthogonal arrangement comes from ensemble fluorescence depolarization spectroscopy (Figure S26) and single-molecule microscopy (Figure S27). Since in the ground state virtually no coupling between the vibrational motion of the two units is expected to occur, the vibrational quanta in the final states of the higher vibronic transitions may be assumed to be localized. It then follows that in the excited state nuclear geometries making the dominant contribution to, e.g., the 0–1 vibronic transition, the molecule must have an asymmetry with one of the chromophores being more distorted along the active vibrational coordinate than the other. If the strength of the electronic coupling between the chromophores is weak relative to the energies associated with the structural relaxation in the excited state relative to the ground state, some asymmetry in the geometry of the molecules can easily induce localization of the excitation on one of the sites.[16] This localization of the excitation can

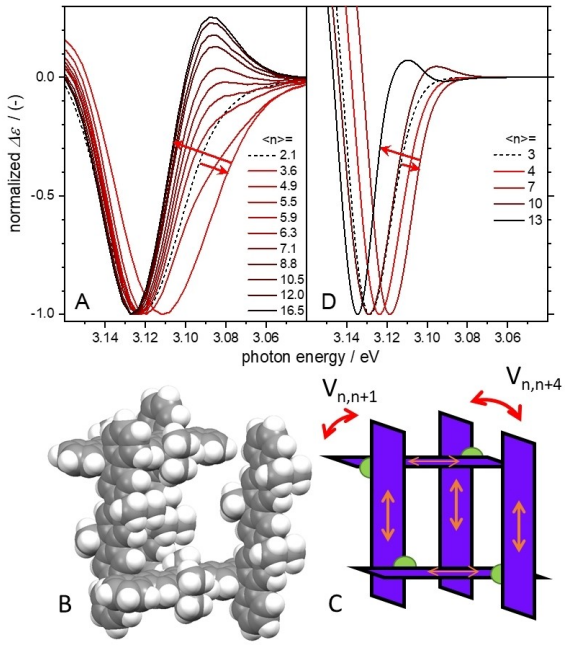

Figure 4. A) Normalized CD spectra near the 0–0 band of the S_1–S_0 transition for narrowly distributed (*S*)-**SBF-LPP$_n$** fractions of different chain length with the average number of monomeric units $<n>$ ranging from 2.1 to 16.5. B) Ground-state conformation as obtained from energy minimization at the AM1 semiempirical level. Evidence for the orthogonal arrangement of chromophores comes from single-molecule and fluorescence depolarization spectroscopy (see Figures S26, S27). C) Schematic depiction of the quantum-mechanical coupled electronic oscillator model indicating the orientation of the transition dipoles and the excitonic couplings included: $V_{n,n+1} = -110\ cm^{-1}$ and $V_{n,n+4} = +200\ cm^{-1}$. The basis set used consists of all possible localized excited states with up to and including 2 quanta of one active vibrational mode with 1600 cm^{-1} frequency and Huang–Rhys factors $S = 0.6$. The green balls indicate the spiro-linkages. D) Simulation of the CD for (*S*)-SBF-LPP for different numbers of monomeric units *n* in the rectangular chain based on the model shown in (C).

then be dynamic in nature and associated with a coupling of electronic and nuclear degrees of freedom in the excited state involving a breakdown of the Born-Oppenheimer approximation. The resulting Herzberg-Teller coupling effect has been investigated in detail in π-conjugated macrocycles using both analytical and numerical techniques.[17] Earlier theoretical analysis has shown that in the limit of very weak electronic coupling between two locally achiral chromophores held in a chiral arrangement, only the 0–0 transition in fluorescence shows any appreciable degree of circular polarization. In this analysis, the 0–1 and higher vibronic transitions featured zero circular polarization in this limit, indicating that asymmetry in the vibrations can completely localize the excitation on one of the chromophores.[10d] This insight is reproduced in section 7 of the Supporting Information. We note that, in the model dimer structure **SBF-LOP**, the two chromophoric groups can interact via the transition dipole—transition dipole mechanism with an estimated interaction energy on the order of $10^2\ cm^{-1}$. Electron exchange between the two quaterphenyl groups is likely small because of the saturated nature of the bridging spiro carbon and the perpendicular orientation of the two chromophores.

To further support our interpretation of the wavelength dependence of the degree of circular polarization in fluorescence, we performed numerical calculations of the quantum-mechanical coupled oscillator model to account for the coupling between electronic and nuclear motion as shown in Figure 4. To reproduce essential features of the fluorescence and absorption spectra we have included two active vibrational modes on the tetraphenyl chromophoric units, one with a frequency of 1600 cm^{-1} and a Huang–Rhys factor $S = 0.60$; and the other at 820 cm^{-1} with $S = 0.39$. The electronic coupling strength V between the chromophores is set to $-110\ cm^{-1}$. This choice reproduces the lower-energy vibronic transitions quite accurately, but due to the limited number of modes included, some of the finer details of the vibronic features at very low transition energies are not rendered accurately. Nevertheless, the overall spectral shape is qualitatively reproduced by the Franck–Condon progression, see Figures 3a,b. This agreement supports the view that there is little if any contribution from excimer-like states involving extensive exchange of electrons between the tetraphenyl units. The g_{lum} values predicted by the quantum-mechanical model are shown as dashed lines in Figure 3c,d. Crucially, the sharp reduction of $|g_{lum}|$ for the higher vibronic transitions compared the 0–0 is reproduced accurately. The reduction of the magnitude of g_{lum} on the high-energy side of the 0–0 transition is also reproduced by taking into account the emission from thermally populated, higher-lying excited states. Here, a simple Boltzmann distribution for the population of excited states is assumed.

The notion of a more localized nature of the higher vibronic transitions in the fluorescence spectra of the pentaphenyl compounds can be further supported by considering the chain-length dependence of the CPL. In comparison to the short dimeric model compounds, the sign of the main g_{lum} extremum in the CPL of **SBF-LPP-C**, in the 0–0 band near 3.1 eV, changes, see Figure 3k,l. The sign of the main g_{lum} extremum is consistent with the sign of g_{abs} in the additional long wavelength CD band, which occurs at the same photon energy. In contrast, sign and magnitude of g_{lum} in the 0–1 vibronic transition near 2.9 eV for the high-molecular-weight polymer is still similar to g_{lum} for the corresponding transition in both the dimeric molecule and the shorter polymer **SBF-LPP-A** bearing stereo centers with the same absolute configuration. This observation indicates that when the polymer is in its lowest excited state, the electronic excitation is delocalized over several (>2) monomeric units, while in the distorted excited state geometries more closely resembling the ground state with one vibrational excitation, the excitation is delocalized over less than two monomeric units. We note that the shape of the fluorescence bands of the polymers further supports this view: while the 0–0/0–1 intensity ratio is very different for the polymer and the dimeric model compound, the 0–1/0–2 intensity ratio is quite similar.[18]

In order to understand the lower excited states in the longer polymers in more detail we have modeled the

evolution of the CD in the long-wavelength region including vibronic coupling with one active vibration with 1600 cm^{-1} frequency. In the square helical conformation adopted, the transition dipole moments of the (uncoupled) individual pentaphenyl monomeric units make right angles with each other and with the helical axis, see Figure 4. In the model we include excitonic coupling between nearest neighbors along the chain ($V_{n,n+1} = -110\ cm^{-1}$) and in space ($V_{n,n+4} = +200\ cm^{-1}$). A new CD band with positive sign is predicted when the chain length exceeds ≈7 units (Figure 4d), consistent with the long wavelength CD band at 3.09 eV in the experimental spectra for the *S*-enantiomer (see Figure 4a). Furthermore, the energy at which the main minimum in CD occurs is predicted to shift to lower photon energies with increasing chain length when $2 < n < 7$. In contrast, when the number of repeat units exceeds 7, the main minimum is calculated to shift to higher photon energies with increasing length. This trend qualitatively reproduces the striking experimental observation of a red shift occurring with increasing molecular weight for $n < 4$ and a blue shift for $n > 4$ (see Figure 4a). The model calculations also predict the appearance of positive g_{lum} in the region of the 0–0 emission band for the *S*-enantiomer for long polymers ($n \approx 10$), while maintaining a negative g_{lum} of almost constant magnitude for the higher vibronic transitions, consistent with the experiment.

Conclusion

Advances in polymer synthesis now allow for construction of π-conjugated helical macromolecules with defined stereochemistry, highly rigid structure and reduced internal degrees of freedom associated with torsional motion between monomeric units. These compounds offer the possibility of detailed study of their excited states. The optical spectra for the square helical polymers investigated here provide experimental support for the notion of dynamic localization of the lowest excited state occurring. The spectra simultaneously show features indicative of a delocalized nature as well as of a localized character of the excited state. The spectral region near the onset of absorption and emission relates to the extended form of the excited state and may thus provide information on long-range order. In contrast, the higher-order vibronic bands relate to the localized form of the excited state and relay information on the structural organization on shorter length scales. The paradigm of dynamic localization may therefore allow for the extraction of more detailed structural information from the spectra of helical macromolecules. In practical terms this will at first involve identifying regions in the CD spectra of biomacromolecules that cover the 0–0 band of particular electronic transitions. Secondly, such spectroscopic features may be further correlated to a higher order structural organization within the biopolymers, for example with respect to their tertiary structure.

Supporting Information: synthesis (including crystallographic and NMR data), chiral separations and chiroptical characterization procedures as well as information on the quantum chemical modelling and supplementary fluorescence depolarization and single-molecule spectroscopy.

Acknowledgements

E.S. and S.S. thank Dr. Jakob Schedlbauer for assistance with the measurements. Financial support from the DFG (project LU 881/10-1, SCHE 410/44-1) is greatly acknowledged. C.W.L. thanks Dr. Sofiane Saouane, beamline scientist P11 for support during remote access.

Conflict of Interest

The authors declare no conflict of interest.

Data Availability Statement

The data that support the findings of this study are available from the corresponding author upon reasonable request.

Keywords: Chirality · Circular Dichroism · Circular Polarization of Luminescence · Helical Ladder Polymers · Spiro Bisfluorene Linkers

[1] R. W. Woody, *Monatsh. Chem.* **2005**, *136*, 347.
[2] a) T. Seidler, M. Andrzejak, M. T. Pawlikowski, *Chem. Phys. Lett.* **2010**, *496*, 74; b) K. A. Kistler, C. M. Pochas, H. Yamagata, S. Matsika, F. C. Spano, *J. Phys. Chem. B* **2012**, *116*, 77; c) M. Deutsch, S. Wirsing, D. Kaiser, R. F. Fink, P. Tegeder, B. Engels, *J. Chem. Phys.* **2020**, *153*, 224104; d) J. Hall, T. Renger, R. Picorel, E. Krausz, *Biochim. Biophys. Acta Bioenerg.* **2016**, *1857*, 115; e) A. F. Fidler, V. P. Singh, P. D. Long, P. D. Dahlberg, G. S. Engel, *Nat. Commun.* **2014**, *5*, 3286; f) A. Troisi, *Phys. Rev. B* **2010**, *82*, 245202.
[3] a) T. Sanematu, *J. Phys. Soc. Jpn.* **1977**, *43*, 600; b) Z. Li, D. Robinson, J. D. Hirst, *Faraday Discuss.* **2015**, *177*, 329; c) D. M. Rogers, S. B. Jasim, N. T. Dyer, F. Auvray, M. Réfrégiers, J. D. Hirst, *Chem* **2019**, *5*, 2751.
[4] a) A. Hanes, Y. Zhang, B. Kohler in *DNA Photodamage* (Ed.: R. Improta, T. Douki), Royal Society of Chemistry, Cambridge, **2021**, pp. 77–104; b) R. Improta, F. Santoro, L. Blancafort, *Chem. Rev.* **2016**, *116*, 3540.
[5] R. Seto, Y. Koyama, K. Xu, S. Kawauchi, T. Takata, *Chem. Commun.* **2013**, *49*, 5486.
[6] Z. Yi, H. Okuda, Y. Koyama, R. Seto, S. Uchida, H. Sogawa, S. Kuwata, T. Takata, *Chem. Commun.* **2015**, *51*, 10423.
[7] T. Ikai, T. Yoshida, K.-I. Shinohara, T. Taniguchi, Y. Wada, T. M. Swager, *J. Am. Chem. Soc.* **2019**, *141*, 4696.
[8] W. Zheng, T. Ikai, E. Yashima, *Angew. Chem. Int. Ed.* **2021**, *60*, 11294; *Angew. Chem.* **2021**, *133*, 11394.
[9] a) T. R. Nelson, A. J. White, J. A. Bjorgaard, A. E. Sifain, Y. Zhang, B. Nebgen, S. Fernandez-Alberti, D. Mozyrsky, A. E. Roitberg, S. Tretiak, *Chem. Rev.* **2020**, *120*, 2215; b) I. Franco, S. Tretiak, *J. Am. Chem. Soc.* **2004**, *126*, 12130.
[10] a) F. C. Spano, S. C. J. Meskers, E. Hennebicq, D. Beljonne, *J. Am. Chem. Soc.* **2007**, *129*, 7044; b) T. Kawai, K. Kawamura, H. Tsumatori, M. Ishikawa, M. Naito, M. Fujiki, T. Nakashima, *ChemPhysChem* **2007**, *8*, 1465; c) R. Tempelaar, A. Stradom-

ska, J. Knoester, F. C. Spano, *J. Phys. Chem. B* **2011**, *115*, 10592; d) F. C. Spano, Z. Zhao, S. C. J. Meskers, *J. Chem. Phys.* **2004**, *120*, 10594.
[11] a) J. Pei, J. Ni, X.-H. Zhou, X.-Y. Cao, Y.-H. Lai, *J. Org. Chem.* **2002**, *67*, 4924; b) R. Tamura, T. Kawata, Y. Hattori, N. Kobayashi, M. Kimura, *Macromolecules* **2017**, *50*, 7978; c) Z. Chen, T. M. Swager, *Macromolecules* **2008**, *41*, 6880; d) D. Qiu, L. Jin, Z. Zheng, H. Meng, F. Mo, X. Wang, Y. Zhang, J. Wang, *J. Org. Chem.* **2013**, *78*, 1923.
[12] Deposition Number 2195804 contains the supplementary crystallographic data for this paper. These data are provided free of charge by the joint Cambridge Crystallographic Data Centre and Fachinformationszentrum Karlsruhe Access Structures service. See Supporting Information for all experimental details.
[13] F. Schindler, J. M. Lupton, J. Feldmann, U. Scherf, *Proc. Natl. Acad. Sci. USA* **2004**, *101*, 14695.
[14] a) L. Brunsveld, R. B. Prince, E. W. Meijer, J. S. Moore, *Org. Lett.* **2000**, *2*, 1525; b) C. C. Chow, C. Chow, V. Raghunathan, T. J. Huppert, E. B. Kimball, S. Cavagnero, *Biochemistry* **2003**, *42*, 7090; c) A. HeténYi, I. M. Mándity, T. A. Martinek, G. K. Tóth, F. Fülöp, *J. Am. Chem. Soc.* **2005**, *127*, 547; d) C. W. Wu, T. J. Sanborn, R. N. Zuckermann, A. E. Barron, *J. Am. Chem. Soc.* **2001**, *123*, 2958.
[15] a) J. L. Greenfield, J. Wade, J. R. Brandt, X. Shi, T. J. Penfold, M. J. Fuchter, *Chem. Sci.* **2021**, *12*, 8589; b) Y. Geng, A. Trajkovska, S. W. Culligan, J. J. Ou, H. M. P. Chen, D. Katsis, S. H. Chen, *J. Am. Chem. Soc.* **2003**, *125*, 14032.
[16] W. T. Simpson, D. L. Peterson, *J. Chem. Phys.* **1957**, *26*, 588.
[17] a) D. Ondarse-Alvarez, T. Nelson, J. M. Lupton, S. Tretiak, S. Fernandez-Alberti, *J. Phys. Chem. Lett.* **2018**, *9*, 7123; b) P. Wilhelm, J. Vogelsang, N. Schönfelder, S. Höger, J. M. Lupton, *Phys. Rev. Lett.* **2019**, *122*, 057402.
[18] F. C. Spano, *Acc. Chem. Res.* **2010**, *43*, 429.

Manuscript received: August 12, 2022
Accepted manuscript online: November 8, 2022
Version of record online: December 2, 2022